Design and Implementation of a High-Efficiency On-Board Battery Charger for Electric Vehicles with Frequency Control Strategy

Jong-Soo Kim, Gyu-Yeong Choe, Hye-Man Jung, Byoung-Kuk Lee
Information and Communication Engineering
SungKyunKwan University
Suwon, Korea
sniper75@skku.edu, lovesagaji@skku.edu,
jungicarus@skku.edu, bkleeskku@skku.edu

Young-Jin Cho, Kyu-Bum Han
EVT Group, R&D Center
Samsung Electro-Mechanics
Suwon, Korea
yj1996.cho@samsung.com,
kyubum.han@samsung.com

***Abstract*— This paper presents a design and implementation of 3.3 kW on-board battery charger for electric vehicles or plug-in hybrid electric vehicles. A series-loaded resonant dc-dc converter and frequency control are adopted in consideration of efficiency, reliability, volume, cost, and so on. In order to obtain high efficiency and less volume within 6 liters, a prototype of the charger is designed and implemented by using high frequency of 80-130kHz and zero voltage switching method. The experimental result indicates 93% of the maximum efficiency and 5.84 liters in volume of the developed 3.3 kW on-board battery charger.**

Keywords-fuel cell electric vehicle; FCEV; low frequency current ripple; fuel cell; driving condtion

I. Introduction

Some of major cities in the world such as Paris, London, Seoul and California, formulates a policy and encourages popularizing an eco-friendly vehicle, typically Electric Vehicles (EVs) and Plug-In Hybrid EVs (PHEVs). In order to speed up its commercial launching in the market, it is necessary to obtain a high-efficiency battery and its charger technology, which is the key power source of the vehicles. Among of various batteries, Nickel Metal Hydride (Ni-MH), Lithium-Ion (Li-Ion) and Li-Polymer batteries are mostly being used to have better energy density, efficiency, safety and cost, and the batteries performances are improving. For the battery charger, two different types of charger are considered, that is, a high speed battery charger with large-capacity (>50 kW) and a on-board battery charger (3.3 kW) that can be used in house electricity.

Especially, an on-board battery charger has to be small and light in order to maximize energy efficiency and the distance covered per charging [1]. Therefore, a high frequency switching technique is required to reduce size of passive components, and to minimize switching losses caused by the high frequency switching, a various zero-voltage-switching (ZVS), zero-current-switching (ZCS) technology by using resonant characteristic, such as series-loaded, parallel-loaded, series and parallel-loaded, resonant-switch and etc., are usually considered [2],[3]. The battery charging algorithm point of view, various researches are performed to have better battery charging algorithm, for instance, Constant Voltage (CV), Constant Current (CC), CC-CV, power control and pulse injection method and so on, considering lifecycle, safety and efficiency of the batteries [4],[5].

In this paper, among of various resonant dc-dc converters, a series-loaded resonant full-bridge dc-dc converter that has benefit in charging for a Li-Ion of 20 Ah for EVs is adopted, and its design and implementation are described in details. In addition, a CC-CV dual-mode battery charging algorithm, which is optimized for Li-Ion battery, is realized by frequency control method by using resonant characteristic. The developed 3.3 kW on-board battery charger achieves 93 % of the maximum efficiency and a Power Factor Correction (PFC) composed by a single-phase rectifier bridge and boost converter reaches up to 0.995 of power factor.

II. System Configuration and Control Strategy

A. System configuration and basic theory

In order to obtain the small, light and high efficiency 3.3 kW on-board battery charger, series-loaded resonant dc-dc converter with full-bridge type is adopted. Entire system consists of EMI filter, diode rectifier, PFC and series-loaded resonant dc-dc converter with full-bridge as shown in Fig.1.

The maximum power of charger reaches up to 3.3kW and this can be considered as a huge load similar with power restrictions of household in case of Korea. Therefore, a power factor of input current has to be compensated according to IEC1000-3-4 Class A regulation because the input current generates a huge harmonics when a simple diode rectifier is used. A boost converter is adopted in PFC in order to improve power factor of input current and to have regulation of output voltage. There are several ways to design PFC such as Boundary mode, Peak current control, DCM, CCM, and etc. In this paper, the Continuous Current Mode (CCM) is used which allows a smaller design in size by reducing input filter dependency and relatively low rms value of current.

978-1-4244-8218-4/10/$26.00 ©2010 IEEE

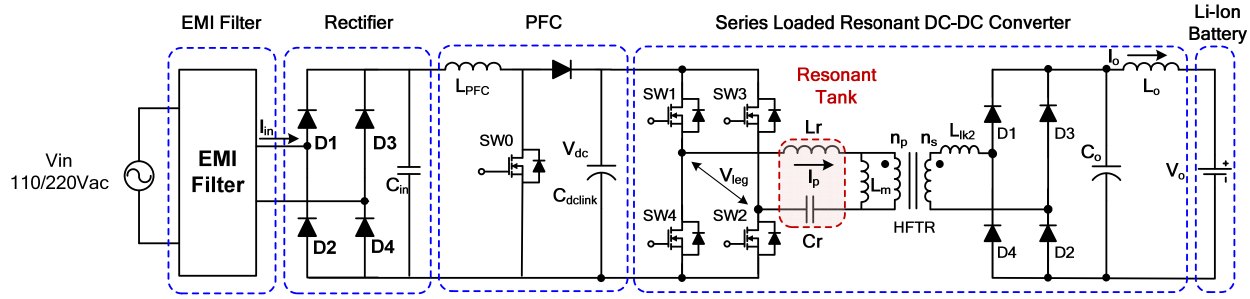

Fig. 1. System configuration comprised of PFC and series-loaded resonant dc-dc converter of the developed 3.3kW battery charger.

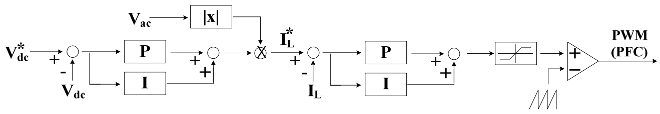

Fig. 2. Control block diagram of PFC.

A control scheme for PFC with CCM is depicted in Fig. 2. A current reference is generated multiplying a voltage controller of outer-loop by an absolute value of input voltage shape. An inner-loop current controller generates pwm reference though comparing current reference and feedback value of inductor current.

For a dc-dc converter, to reduce the size of 3.3 kW on-board charger intended for use in EVs, it is desirable to increase the operating frequency to reduce the size of passive components. For a consideration, to reduce an additional switching loss due to the increased switching frequency, we adopt a series-loaded resonant dc-dc converter. This converter has a series topological structure that consists of resonant inductor and capacitor, and load resistor. Fig. 3 shows an ac equivalent circuit and a resonant characteristic of the resonant converter [6],[7].

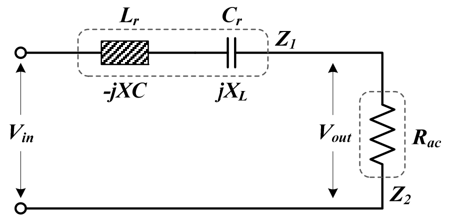

(a) Equivalent circuit of series-loaded resonant dc-dc converter

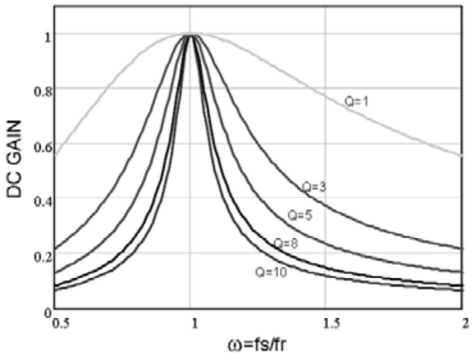

(b) Gain characteristics according to Q-factor and switching frequency

Fig. 3. AC equivalent circuit for series-loaded resonant dc-dc converter.

An in-out gain of a series-loaded resonant dc-dc converter can be expressed by using the equation for a voltage divider between Z_1 and Z_2.

$$\frac{V_{out}}{V_{in}} = \frac{1}{1 + j\left[\frac{X_L}{R_{ac}} - \frac{X_C}{R_{ac}}\right]} \tag{1}$$

where, $R_{ac} = 8R_L / \pi^2$.

And, Q-factor is

$$Q = \frac{\sqrt{L_r / C_r}}{R_L} \tag{2}$$

Therefore, final converter gain being given by

$$\frac{V_{out}}{V_{in}} = \frac{1}{1 + j\frac{\pi^2}{8}Q\left[\frac{\omega}{\omega_0} - \frac{\omega_0}{\omega}\right]} \tag{3}$$

where, $\omega_0 = 1/\sqrt{L_r C_r}$

As in eq. (3), the output voltage of the converter varies according to switching frequency and load condition. Thus, in case of battery charger application, we can achieve the desired output current and voltage through frequency control even though equivalent resistance of a battery is changed according to charging status.

B. *Frequency control scheme*

For charging algorithm, dual-modes charging strategy with a combination of CC and CV as shown in Fig. 4(a) to obtain more efficient Li-Ion battery charging is applied.

A charging current reference (I^*_{batt}) is generated by voltage control of outer-loop, and inner-loop current controller controls charging current as shown in Fig. 4(b). When state-of-charge (SOC) of Li-Ion battery is low, the I^*_{batt} is increased and operate in CC mode above a preset limiter value. When SOC is increasing, the I^*_{batt} is decreased and the control algorithm changes to CV mode once the I^*_{batt} goes below

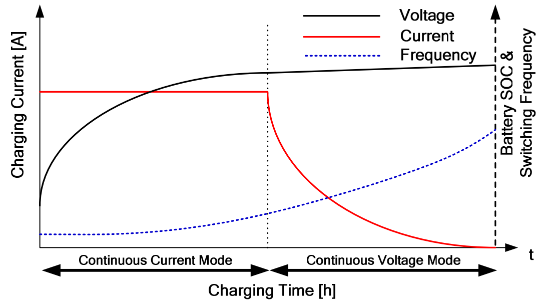

(a) Battery charging strategy according to SOC with frequency control.

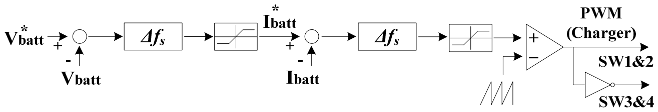

(b) Optimal frequency tracking scheme

Fig. 4. Control scheme for battery charging.

than the preset limiter value. The final PWM is a fixed-duty and variable frequency, and a switching frequency command is generated by output of the current controller. A determination of charging mode depends on battery management system (BMS) and characteristic curve of Li-Ion battery.

III. Design and Implementaion of Battery Charger

In this section, design and implementation of the developed 3.3 kW on-board battery charger are described in details.

The first step for the system design, a resonant frequency of series-loaded resonant dc-dc converter is designed to f_r*=71.6 kHz (*L_r*=75 uH,* C_r*= 66 nF)* by considering the size and switching losses of passive complements. In this condition, resonant characteristic is shown as Fig. 5(a). A controller is designed to perform an optimal frequency tracking control between f_{sw}=80-130 kHz to have 250-410 V of output voltage that fits in Li-Ion battery characteristic. An output current and voltage is controlled by the proposed charging algorithm in accordance with switching frequency causing change of valid output energy density as shown in Fig. 5(b). The detail system parameters are listed in table I.

TABLE I
System Parameters

Parameters	Value [Unit]
Rated Power	3.3 [kW]
Input Voltage	100-277 (+/-10%) [V_{rms}]
Output Voltage	250-410 (+/-2V) [V_{dc}]
Resonant L & C	150 [uH] & 33 [nF]
PCB Dimension	228x338 [mm]
Output Current	10 (+/-10%) [A]
Ripple Voltage	< 25 [V_{pp}]
Ripple Current	< 10% from $I_{nominal}$
Switching Frequency	80-130 [kHz]
Entire System Volume	5.84 [L]

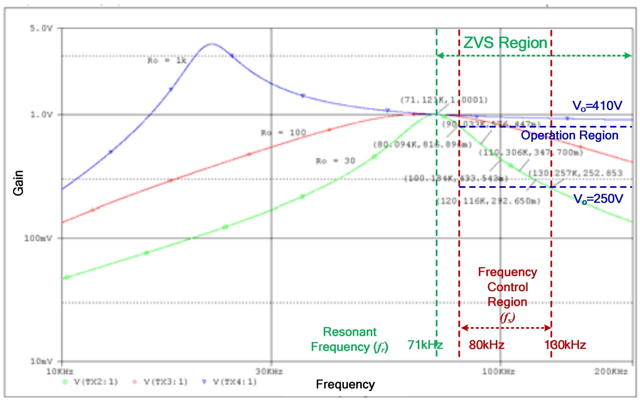

(a) Gain characteristic according to frequency and operation region.

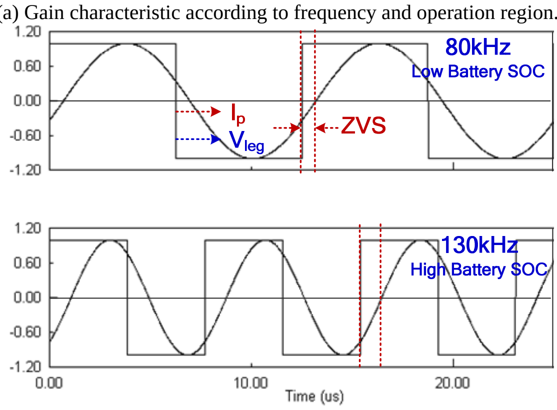

(b) Leg voltage and resonant current according to switching frequency.

Fig. 5. Resonant characteristic curve and typical waveform.

A. *Design of active componnents*

A voltage rating of diode and MOSFET has to be designed considering the peak value across anode-cathode voltage of the diode and drain-source voltage of the MOSFET at turn-off. Moreover, if the blocking voltage of the power semiconductor switches gets over the reverse bias safety operation area (RBSOA), the switches are totally destroyed by thermal runaway due to avalanche effect. The RBSOA is reduced by stray inductance of a PCB patter or a connection wire as well as internal stray inductance of the switches. Thus, the voltage margin should be considered. However, too much margin brings out increase of conduction loss due to a gain in V_F, $V_{ce(sat)}$, R_{DSon}, etc. Consequently, diode and MOSFET 600 V class of are selected as follows:

$$V_{rated} \geq k \cdot \left(V_{pp} + L_{ts} \frac{di_s}{dt} \right) \qquad (4)$$

where, V_{pp} is peak value, L_{ts} is total stray inductance, and k is safety factor.

A current rating of power semiconductor switches has to be designed to be not over generally 125℃ of junction temperature even overload or abnormal conditions. Thus, an accurate calculation or simulation of power dissipation considering thermal management system inevitably needs to find junction temperature of the switches. The power dissipation of a MOSFET being given by

$$P_{TOT} = P_{sw} + P_{cond} + P_{Coss} + P_{fw} \tag{5}$$

Switching loss is given by

$$P_{sw} = f_{sw}\left[\left(\int_{t_{off}}^{t_{on}} I_D(t)\cdot V_{DS}(t)dt\right) + \left(\int_{t_{on}}^{t_{off}} I_D(t)\cdot V_{DS}(t)dt\right)\right] \tag{6}$$

where, $t_{on} = t_{d(on)} + t_r$ and, $t_{off} = t_{d(off)} + t_f$

Conduction loss can be expressed by

$$P_{cond} = I_D^2 R_{DSon} D_{on} \tag{7}$$

The loss due to parasitic output capacitance is

$$P_{Coss} = \frac{C_{oss} V_{in}^2 f_{sw}}{2} \tag{8}$$

And body diode loss during freewheeling mode can derive as follows:

$$P_{fw} = I_{fw} V_F D_{off} \tag{9}$$

Based on calculation results of power dissipation, MOSFETs of 90 A and 50 A classes are selected for PFC and dc-dc converter, respectively, considering low R_{DSon}, E_{on}, E_{off}, and C_{oss}.

A gate driver has to provide a current capability for fast turn-on and turn-off of a MOSFET. Thus, we design a gate driver of 4 A_{peak} current capability from gate charge of MOSFET and applied gate-source voltage. In addition, a gate resistor is selected considering optimal point between switching loss and transient characteristic. The peak current and average current of a drive IC are as follows:

$$I_{g,peak} = \frac{V_{gs}}{R_g} \tag{10}$$

$$I_{g,avg} = Q_g f_{sw} \tag{11}$$

where, V_{gs} is gate-source voltage and R_g is gate resistance.

B. Design of magnetics

A core for PFC is used High Flux core, which has soft saturation and good thermal characteristics, because of wide variation of inductor current compare with a resonant dc-dc converter. The core used for PFC inductor has cross section area of 0.678 cm^2, nominal inductance of 56 nH/N^2, and permeability of 125 μ . A core for series-loaded resonant dc-dc converter is adopted a Ferrite core of PQ5050 type, which has good frequency characteristic, high saturation flux density, constant dc bias characteristic, and high permeability, taking into account a stability of frequency control. A high frequency transformer is designed with a Ferrite core of EE7066 type, and its turn ratio is 19:26 considering in-out specification. An area product for selection of the core is

$$A_W A_E = \left(\frac{10^4 P_{in}}{420 k_t k_u k_p \Delta B 2 f_t}\right)^{1.31} = \frac{11.1 P_{in}^{1.31}}{k\Delta B f_t}[cm^4] \tag{12}$$

where, $P_{in} = P_o/\eta$

$k_t = I_{in,dc}/I_{p,rms} = 1$: topology factor

$k_u = A_w'/A_w = 0.4$: window utilization factor

$k_p = A_p/A_w' = 0.41$: primary area factor

$k = k_t k_u k_p = 0.165$

f_t is transformer operating frequency

Especially, in case of a Feritte core, it has minimal core loss at about 90℃ of core temperature. To obtain high efficiency, optimal design and thermal management were thus performed.

Polypropylene capacitor with metal-foil electrodes has good characteristic for high frequency, so that we select it for resonant capacitor.

C. Design of themal management system

The design target of a thermal management system is also maintaining below 125℃ of the junction temperature for the power semiconductor devices. The power dissipation of a power semiconductor is electrically equivalent to a current source. Fig. 6 indicates an equivalent thermal model for one MOSFET consisting of one switch and one body diode [8].

The maximum junction temperatures of MOSFET and body diode at continuous operation are given by:

$$T_{vj,MOSFET} = T_{amb} + R_{thha}\sum P + R_{thjh}\sum P_{MOSFET} \tag{13}$$

$$T_{vj,FWD} = T_{amb} + R_{thha}\sum P + R_{thjh}\sum P_{FWD} \tag{14}$$

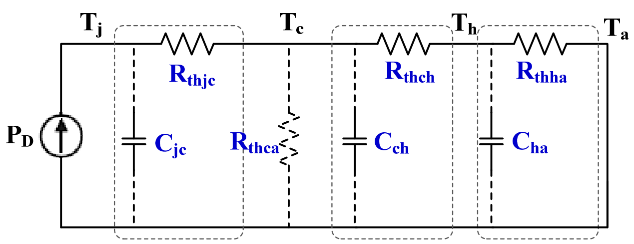

Fig. 6. equivalent thermal model.

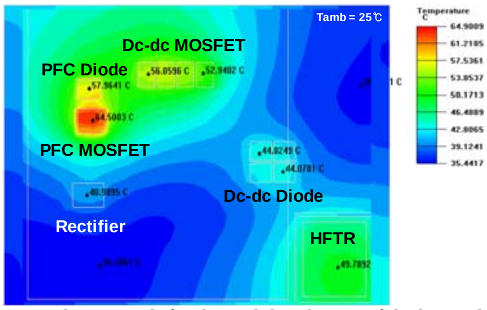

(a) Simulation result for thermal distribution of the heatsink.

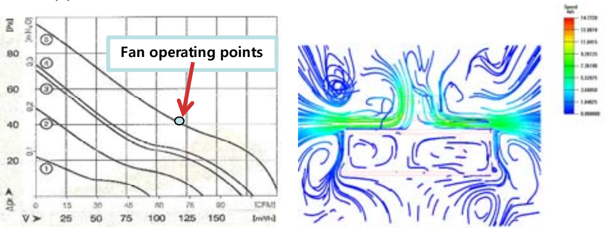

(b) Operating characteristic of fan and air fluid analysis.

Fig. 7. Simulation and analysis results for thermal characteristics of heatsink.

The simulation result of thermal distribution of the heatsink and analysis result of air fluid with a fan are performed using IcePack of thermal design program, and these are shown in Figs. 7(a) and (b). As results of a calculation and a simulation of power dissipation, a MOSFET for PFC having serious loss is placed the nearest fan, which has an abundant air fluid. The highest temperature on the heatsink is about 64.5℃ under 25℃ of ambient temperature. Considering 60℃ of ambient temperature, the junction temperature of the MOSFET for PFC is limited to under 125℃.

D. Design of digital controller

A digital controller of DSP 320F28335 from TI is used for entire system control and charging current control. The main clock of the DSP is set with 150MHz, so that we can get a frequency control resolution of 69.3 Hz / step. And a battery has extremely low dynamics. Therefore, we can control the charging voltage and current using digital controller without the help of any analog circuit.

E. Hardware realization

A 3D mechanical design was performed for an accurate hardware design. To realize more small and effective radiation of heat, heatsink and case are designed with all-in-one. Figs. 8(a) and (b) show the mechanical 3D drawing and the realized battery charger.

IV. EXPERIMENT RESULT

The performance test of the developed battery charger was carried out with an ac power supply of 6 kW and an electronic load of 3.6 kW. The measurement of the efficiency, power factor, voltage and current was used power analyzer WT3000, and temperature was measured by MV2000. The entire experiment setup is shown in Fig. 9.

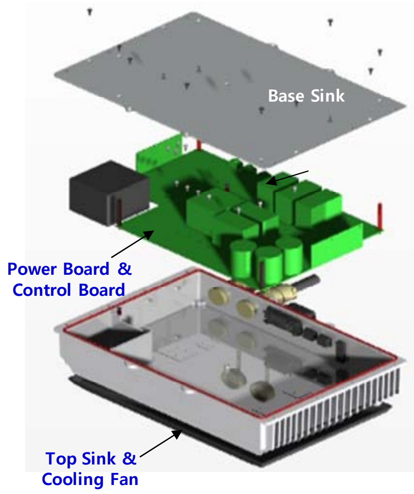

(a) 3D design of 3.3kW on-board battery charger for EVs .

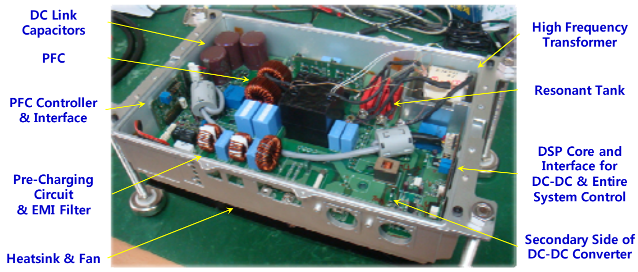

(b) Picture of 3.3kW on-board battery charger for EVs .

Fig. 8. Mechanical 3D design and picture of the developed 3.3kW on-board battery charger.

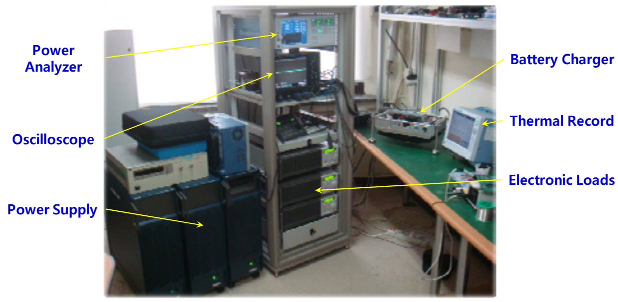

Fig. 9. Experiment setup.

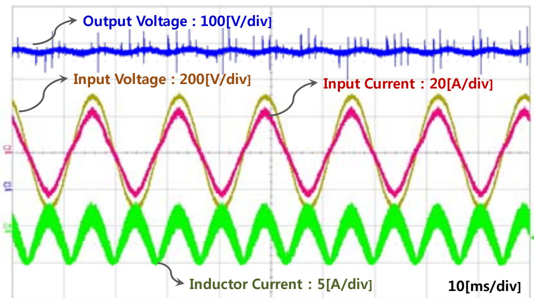

Fig. 10. Experiment waveforms of PFC at full load condition of 3.3kW.

The PFC test waveform at rated power condition is shown in Fig. 10. The output voltage is controlled at the level of 380V

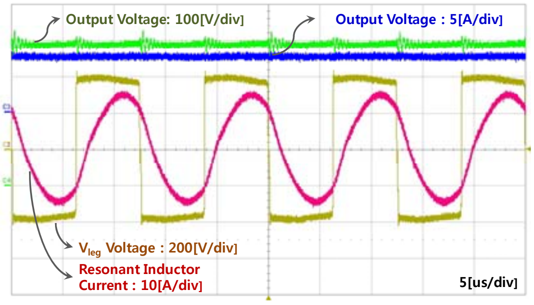

(a) Leg voltage (V_{leg}), resonant current (I_p) and output voltage and current of dc-dc converter at 80 kHz of switching frequency.

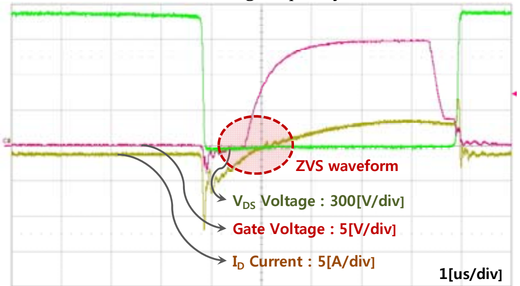

(b) ZVS characteristic at 80 kHz condition.

Fig. 11. Experiment waveforms of series-loaded resonant dc-dc converter at full load condition of 3.3kW.

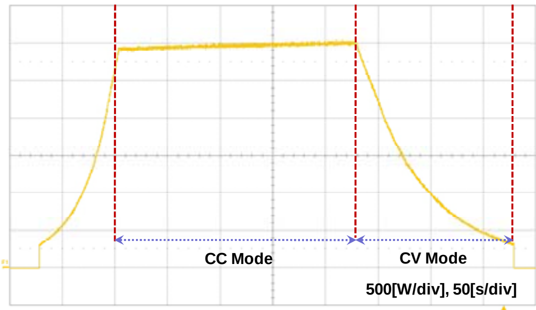

Fig. 12. Simulated battery charging test with CC-CV scheme.

and the input current is well controlled as sine wave, as a result, it is achieved 0.995 of power factor.

The test results of the series-loaded resonant dc-dc converter under the identical condition with the PFC are shown in Figs. 11(a) and (b). Fig. 11(a) shows that the voltage and current are controlled 400 V of output voltage with about 20V ripple and 7.9 A of current with about 0.1 A ripple, respectively. Fig. 11(b) shows ZVS characteristic from gate-source voltage, drain current and leg voltage (V_{leg}) of a MOSFET for dc-dc converter at 80 kHz switching frequency. This experiment result shows that ZVS is assured at minimum switching frequency. Fig. 12 shows a result of simulated battery charging test from 3 kW with CC-scheme during 4min to 0 W with CV-scheme during 3min. The waveform indicates the output power, and it also well controlled. The test efficiency and power factor according to the input power are shown in Fig. 13.The minimal and maximal efficiencies of the developed battery charger system are 84 % at 300 W and 93 % at 2.7 kW, respectively.

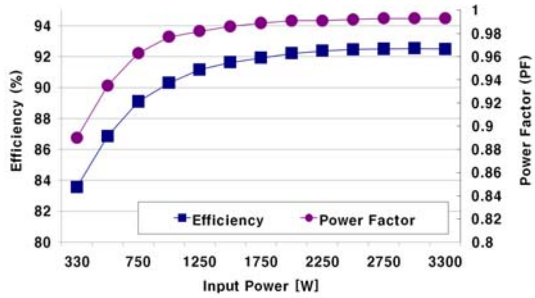

Fig. 13. Control strategy for battery charging.

V. Conclusion

This paper presents a topological structure and control strategy of 3.3 kW on-board battery charger system for EVs and PHEVs. The hardware of 3.3 kW on-board charger was designed and implemented by using the series-loaded resonant dc-dc converter and frequency control strategy, and achieved 93% of efficiency and 0.995 of power factor. In addition, the developed charger was realized 5.84 liters in volume with a smaller heatsink and smaller passive components that those were achieved by reducing the switching loss through ZVS and by using high frequency switching. It is expected that the developed on-board charger can be good solution for the eco-friendly vehicles. For the next version of this paper, the charging algorithm will be verified by experiment using Li-Ion battery.

References

[1] M. M. Morcos, C. R. Mersman, G. G. Sugavanam, and N. G. Dillman, "Battery chargers for electric vehicles," *IEEE Power engineering Review*, pp. 8-11, November 2000.

[2] Y. C. Chiang, Y. L. Ke, H. S. Chuang, and H. K. Chen, " Implementation and analysis of an improved series-loaded resonant dc-dc converter operating above resonance for battery chargers," *IEEE Industrial and Commercial Power Systems Technical Conference (ICPS) 2008*, pp. 1-8, May 2008.

[3] Y. C. Chuang and Y. L. Ke, "High-efficiency and low-stress ZVT-PWM DC-to-DC converter for battery charger," *IEEE Trans. Ind. Electron.*, vol. 55, no. 8, pp. 3030-3037, August 2008.

[4] J. J. Chen, F. C. Yang, C. C. Lai, Y. S. Hwang, and R. G. Lee, " A high-efficiency multimode Li–Ion battery charger with variable current source and controlling previous-stage supply voltage," *IEEE Trans. Ind. Electron.*, vol. 56, no. 7, pp. 2469-2478, July 2009.

[5] S. Y. Tseng, T. C. Shin, S. Y. Fan, and G. K. Chang, " Design and implementation of lithium-ion/lithium-polymer battery charger with impedance compensation," *IEEE International Conference on Power Electronics and Drive Systems (PEDS) 2009*, pp. 866-870, November 2009.

[6] R. L. Steigerwald, "A comparison of half-bridge resonant converer topologies," *IEEE Trans. Power. Electron.*, vol. 3, no. 2, pp. 174-182, April 1988.

[7] N. Mohan, T. M. Undeland, W. P. Rbbins, "Power electronoics converter, application and design," 3rd ed., John Wiley & Sons, Inc., 2003.

[8] U. Nicolai, T. Reimann, L. Petzoldt, J. Lutz, "Application manual power modules," SEMIKRON International, [Online]. Available: http://www.semikron.com/skcompub/en/application_manual-193.htm.